Computational study of phonon modes in short-period AlN/GaN superlattices

Tula R. Paudel and Walter R. L. Lambrecht
Department of Physics, Case Western Reserve University, Cleveland, Ohio 44106-7079, USA
(Received 22 July 2009; published 28 September 2009)

The phonons and infrared absorption of short period [0001] superlattices $(AlN)_n(GaN)_{8-n}$, with $n=3,4,5$ were calculated by using the density-functional perturbation theory in the local-density approximation. The nature of the modes is discussed in terms of quantum confinement and interface localized modes. The spectrum for *e*-symmetry modes shows two TO peaks, of which the lowest corresponds to two closely spaced modes confined each near one half of the GaN part of the cell, and the higher one to two closely spaced AlN like modes with one mode localized at the interface showing the strongest oscillator strength and a bulklike LO-TO splitting. For a_1 symmetry, in contrast, a GaN vibration type mode localized near the interface shows the strongest LO-TO splitting and oscillator strength, while two higher modes are found to be only weakly localized in the AlN part of the cell. Lattice constant relaxation of free-standing superlattices leads to a decreasing lattice constant with increasing number of AlN layers and hence an overall increase in phonon frequencies. Qualitative agreement with experimental data is found for the *e* symmetry but quantitative discrepancies exist and are interpreted as evidence of a different strain state in the experiment.

DOI: 10.1103/PhysRevB.80.104202 PACS number(s): 68.65.Cd, 68.65.Ac, 78.30.−j, 74.25.Kc

I. INTRODUCTION

The study of phonons in superlattices has attracted attention ever since it became possible to grow semiconductor superlattices of high quality. Folded acoustic modes confined optical modes as well as interface localized modes have been observed and discussed abundantly.[1] For relatively long period superlattices, semiclassical models can be applied. On the other hand, in very short period superlattices it becomes imperative to treat these materials effectively as new compounds and include the details of the atomic relaxations. It becomes somewhat doubtful if classical concepts such as interface localized modes and confined modes are still applicable. Do the barriers inhibiting the propagation of certain modes and leading to confinement still stay effective for very thin layers or do the phonons somehow tunnel through these thin barriers? The study of very short period superlattices is also related to that of phonons in disordered alloys. In the latter case, one can distinguish one-mode from two-mode behavior and the bond-length distribution was found to play an essential role.[2] It is thus of interest to compare this behavior with that in short-range superlattices where bond length variations are bound to occur as one moves from the bulklike regions toward the interface.

Among semiconductor superlattices, the AlN-GaN superlattices present a specific challenge. Unlike AlAs and GaAs which have well separated optic phonon bands and thereby provide a classic example of mode confinement, the optical phonon bands of AlN and GaN overlap significantly in their frequency ranges. For example, for GaN, the optical phonons range from about 550–750 cm^{-1}, whereas for AlN they extend from about 610–920 cm^{-1}. See, for example, Ref. 3 for full phonon-dispersion spectra. AlN and GaN are also strongly polar materials with large ionicity and accompanying large LO-TO splittings, spontaneous polarization, and piezoelectric strain induced electric fields, which may influence the phonon behavior.

Recently, Mintairov *et al.*[4] performed an infrared reflectivity study of the phonon modes in $(AlN)_4(GaN)_4$ superlattices providing further motivation for a computational study. Here we present calculated phonons and infrared spectra of $(AlN)_n(GaN)_{8-n}$ superlattices with $n=3,4,5$. We examine the three types of superlattices to study the effects of the thickness of the AlN layer, and also because in experimental superlattices, atomic scale fluctuations of the layer thickness may occur. Our aim at this stage is not a one-to-one correspondence to the experimental spectra but rather to gain qualitative insights in the nature of the phonons in these structures.

II. COMPUTATIONAL METHOD

The calculations were carried out using the linear-response approach[5–7] together with an iterative minimization norm-conserving pseudopotential plane-wave method[6–8] and within the framework of density-functional theory[9,10] as implemented in the ABINIT package.[11] The local-density approximation was used for the exchange and correlation energy.[12] In the Fritz-Haber pseudopotentials we used,[13] the semicore Ga 3*d* electrons are treated as valence electrons. The calculation for pure AlN and GaN are carried out with kinetic-energy cutoff of 70 Ry and $6\times6\times6$ regular shifted *k*-point meshes. The calculations for superlattices were carried out with 70 Ry plane-wave energy cutoff and the orthorhombic Brillouin zone was sampled with a regular and shifted $6\times6\times3$ *k*-point mesh. The calculation is well converged as increasing plane-wave cutoff to 80 Ry and of the *k*-points mesh to $8\times8\times4$ yields on average to less then a percent change in phonon frequencies.

III. RESULTS

In this section we present the results of our calculation in five different subsections. In Sec. III A we present results for the phonon modes of pure AlN and GaN at the Γ point. Although the phonon modes in pure AlN and GaN have been extensively studied in the literature, both theoretically[3,14–19]

and experimentally[20–22] it is important to validate our computational method and for comparison of the superlattice modes to those of the individual materials. Next (in Sec. III B) we present the phonon frequencies and the nature of the vibrational modes as well as the infrared spectra of the $(AlN)_4(GaN)_4$ superlattice. In Sec. III C we discuss the changes in these spectra induced by layer thickness variation. We present our results for the static and high-frequency dielectric tensors in Sec. III D. Finally, in Sec. III E we compare our results with the experimental data of Mintairov *et al.*[4]

A. Zone-center phonons of AlN and GaN

The equilibrium structure of both AlN and GaN is the wurtzite structure which corresponds to the space group C_{6v}^4. For the phonons at the Γ point, we only need the point group C_{6v}. One can classify the 12 phonons in these compounds according to the irreducible representations A_1, B_1, E_1, and E_2. Out of these, A_1 and E_1 are infrared active because they couple to electric fields along the c axis and perpendicular to the c axis, respectively. The modes of A_1, E_1, and E_2 symmetries are also Raman active, while the B_1 modes are silent. The infrared inactive E_2 and B_1 irreducible representations each contain two modes: a low-frequency (acoustic) region and a high-frequency (optical) region one.

As is well known, A_1 and B_1 modes both correspond to vibrations along the c direction. However for the silent B_1 modes the two cation-anion pairs in the cell move in antiphase with respect to each other. They correspond essentially to a folded mode of the zinc-blende Brillouin-zone L point. The low-frequency mode is a folded acoustic mode in which the two cation-anion pairs as a whole move against each other in the z direction, while the high-frequency mode involves bond stretches of each cation-anion pair but with opposite sign for the two pairs in the cell. The A_1 optical mode corresponds directly to a bond-stretch mode of the cation-anion bonds parallel to the c axis with the same sign for both molecules. Similarly, the doubly degenerate E_2 modes have opposite sign for the two molecules in the cell while the E_1 mode has the same sign. These correspond to in-plane vibrations in x or y direction.

We compare our calculated phonon frequencies for AlN and GaN with experimental data in Table I. Excellent agreement is observed for both.

TABLE I. Calculated zone-center phonon frequencies (in cm^{-1}) in AlN and GaN compared with experimental data.

Compound	Mode	Calculated	Experimental
AlN	E_2^{low}	246	252[a]/241[b]
	B_1^{low}	552	
	A_1^{TO}	613	614[a]/607[b]
	A_1^{LO}	882	895[a]
	E_2^{high}	665	660[a]
	E_1^{TO}	676	673[a]
	E_1^{LO}	921	
	B_1^{high}	737	
GaN	E_2^{low}	136	145[c]
	B_1^{low}	331	
	A_1^{TO}	533	533[c]
	A_1^{LO}	724	724[c]
	E_2^{high}	561	660[c]
	E_1^{TO}	555	561[c]
	E_1^{LO}	720	742[c]
	B_1^{high}	687	

[a]McNeil *et al.* (Ref. 20).
[b]Perlin *et al.* (Ref. 21).
[c]Filippidis *et al.* (Ref. 22).

B. Phonons in 4+4 superlattice

We here consider a 4+4 superlattice in the [0001] direction. This supercell has 16 atoms per unit cell and 48 phonon modes. The symmetry of the superlattices is reduced to C_{3v}. The modes can be divided into $16a_1$ and 16 doubly degenerate e modes using the point-group symmetry C_{3v}. This includes a zero-frequency translation mode of each symmetry so we have 15 modes of each symmetry do deal with. Of these eight modes correspond to the optical modes of the parent compounds, while seven modes are folded acoustic modes. We will use lower case to indicate the irreducible representations of the C_{3v} group so as not to confuse them with the wurtzite mode symmetries. In comparison with the modes of the individual wurtzite materials, a_1 comprises both A_1 and B_1 and e modes comprise both E_1 and E_2. The a_1 modes couple to an electric field in the z direction (along the c axis of the structure) while the e modes couple to electric fields in x and y directions. Thus all modes are infrared active and exhibit TO-LO splitting.

In Table II we present the zone center modes of the 4

TABLE II. Zone center phonons in $(AlN)_4(GaN)_4$ superlattice (in cm^{-1}).

e^{TO}	e^{LO}	a_1^{TO}	a_1^{LO}
70	70	143	144
75	75	155	155
119	119	264	264
125	125	287	288
155	155	340	340
201	201	422	423
236	237	507	507
586	588	570	718
590	604	699	699
593	593	710	710
597	597	720	727
614	614	754	754
618	618	780	804
623	625	827	880
628	813	848	848

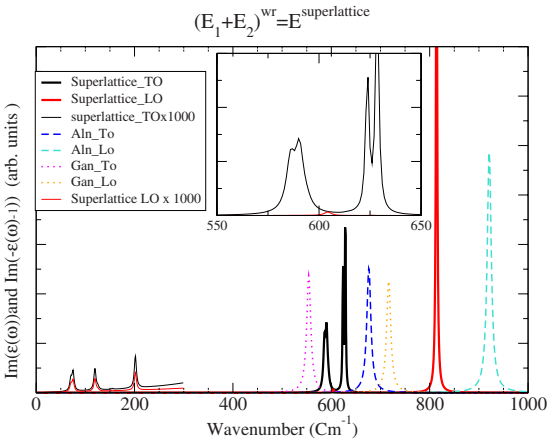

FIG. 1. (Color online) Longitudinal and transverse response of the $(AlN)_4(GaN)_4$ superlattice for *e*-symmetry modes. Low-lying mode are multiplied by 1000 and the TO spectrum between 550–625 cm^{-1} is replotted for better viewing in the inset.

+4 superlattice.

It is clear from Table II that the seven lower phonon modes are folded acoustic modes. They have very small LO-TO splittings and are restricted to the range below 510 cm^{-1} which is below the lowest TO mode in GaN. Of the upper eight modes, which can be viewed as derived from the optic modes in the parent compounds, only two have a large LO-TO splitting (or order 200 cm^{-1}) comparable to those in the parent compound: the modes $a_1(8)$ and $e(15)$. Several modes have weak to intermediate LO-TO splittings of order a few cm^{-1}. Several modes even in the optic range have still negligible LO-TO splitting. This makes sense if they are somehow derived from E_2 or B_1 modes which means they are in antiphase with respect to each other between successive double layers.

Modes with a strong LO-TO splitting also correspond to a strong oscillator strength. The oscillator strengths are calculated as the squared product of the Born effective charges and the eigenvector for each phonon mode. The Born effective charges are calculated as the mixed electric field and atomic displacement derivative of the total energy. The mode eigenvector is obtained by solving the secular equation of the dynamical matrix. The oscillator strength function is then used to calculate the dielectric function by using Eq. (1).

$$\varepsilon_{\alpha\beta}(\omega) = \varepsilon_{\alpha\beta}^{\infty} + \frac{4\pi}{V}\sum_{m}\frac{S_{m,\alpha\beta}}{(\omega_m^2 - \omega^2 - \imath\Gamma_m\omega)}, \qquad (1)$$

where V is the volume of the unit cell, Γ_m is a mode-dependent damping factor, and $\varepsilon_{\alpha\beta}^{\infty}$ is the electronic part of the dielectric function. The peak locations of $\mathrm{Im}[\varepsilon(\omega)]$ give the transverse modes, while the peaks of $\mathrm{Im}[-\varepsilon^{-1}(\omega)]$ gives the longitudinal phonon modes. For lack of knowledge of the damping, we use a mode-independent damping factor.

In Fig. 1 we present the calculated transverse and longitudinal infrared response curves for the 4+4 superlattice compared with those of AlN and GaN for modes of *e* symmetry. Essentially, we see two peaks in the TO spectrum, each split in two. Actually, there are eight modes in this range. From Fig. 2 we can see that the lower 4 modes with frequencies below 600 cm^{-1} predominantly have displacements in the GaN portion of the cell, while the four higher modes are localized in the AlN portion. This is not surprising given that Al is the lighter atom and in comparison with the TO modes in the bulk materials. All of these modes have predominantly displacements of the N atoms as expected for the optical modes although a few show a considerable Al displacement. It is instructive to try to interpret the vibration patterns in terms of confined modes. Looking carefully at the pattern, we can see that the signs of the displacements for the four lower modes in increasing order of energy can be described as: ++00, 00++, +−−+, and +−+−. Here, + and − simply indicate the relative signs of the displacements on successive layers. The lower two can be viewed as bonding and antibonding linear combinations of ++++ with ++−−. Thus, we can in some sense think of these as the expected particle in a box type confined modes with increasing energy. However, it is clear that there are significant interactions between these basic confined mode patterns leading to different amplitudes of the oscillation on different atoms. For example, the lower two become localized respectively near the bottom and top AlN/GaN and GaN/AlN interfaces respectively or at least they each localize in only half of the GaN portion of the cell. It turns out that these two lower modes also have the higher oscillator strength. This is because they correspond to two molecules vibrating in phase with each other.

The second peak above 600 cm^{-1} corresponds to modes localized in the AlN part. We can see that the mode patterns from low to high frequency are now −+−+, −+++−, 00++, and ++00. Here we consider the top N atom shown in the figures as part of the AlN portion of the cell because it is triple bonded to Al and only single bonded to Ga. Again, these are confinement mode patterns but they seem to occur in opposite order of the usual one. The lower two of these have almost zero LO-TO splitting and hence oscillator strength. For the highest mode we see a substantial participation of the Al atom. This is the only mode with a clear Al-N bond stretch and in fact this is the mode with a bulklike LO-TO splitting 185 cm^{-1}. This mode is in fact rather localized near the bottom interface, i.e., the GaN/AlN interface that is the interface with N bonded to three Al and one Ga. The mode just below it is instead localized near the AlN/GaN interface, i.e., the interface with a N bonded to three Ga and one Al, occurring in the middle of the cell in Fig. 2. More precisely, this mode is localized in the top half of the AlN portion of the cell.

Comparing with the pure material spectra, we can see that the modes confined in the GaN portion of the cell giving rise to the lower peak occur at a frequency somewhat higher than the bulk GaN frequency. The upper peak occurs at a frequency below that of bulk AlN. This we attribute to the fact that the lattice constants in the plane are relaxed and in between the AlN and GaN ones. Thus GaN bonds are compressed in the plane and their frequencies shift up as expected, while AlN bond are stretched and their frequency is reduced. In the LO or loss spectrum, the only strong peak is as mentioned corresponding to a interface localized mode with strong AlN character. Thus, in some sense we see two-

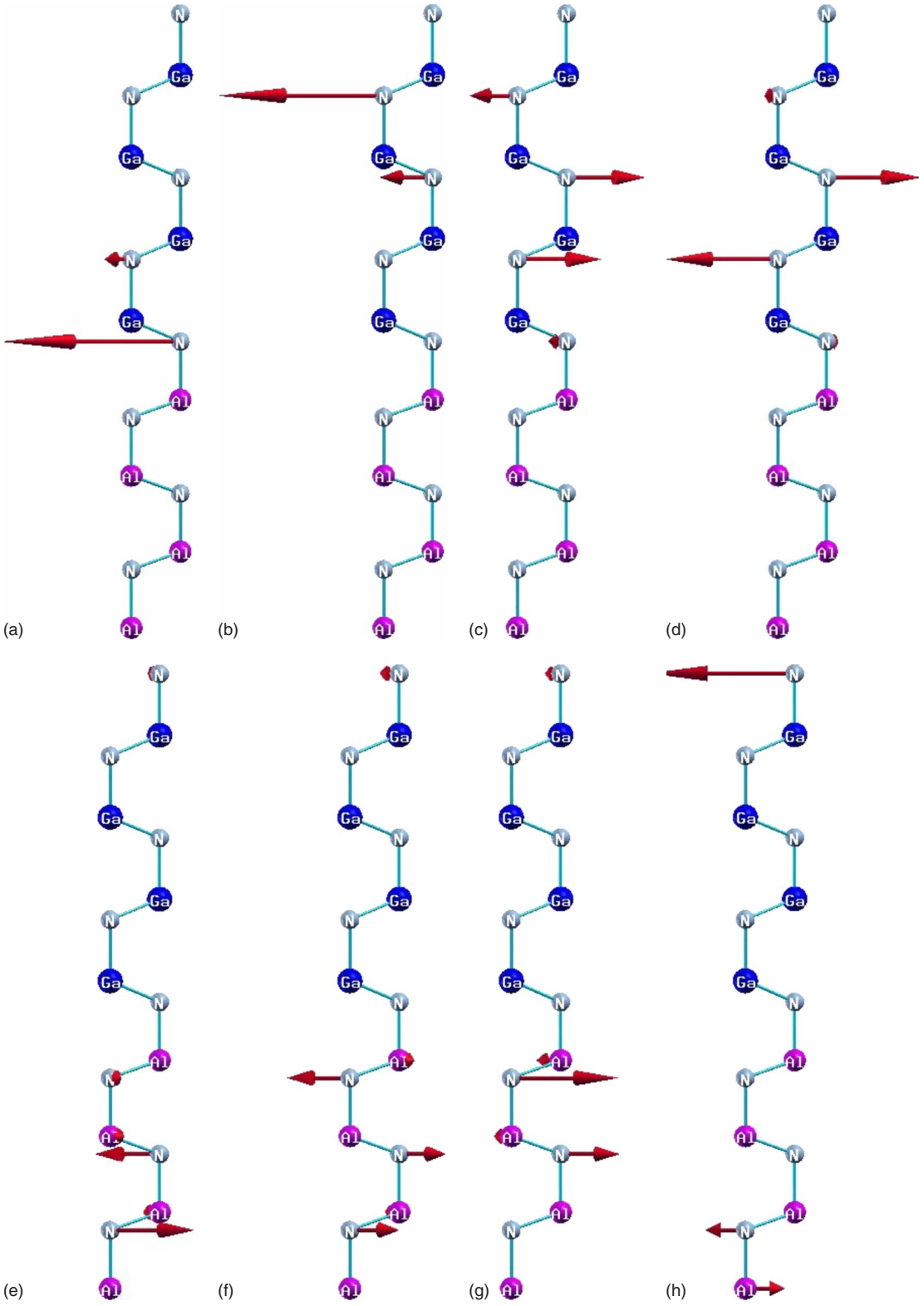

FIG. 2. (Color online) From upper left to lower right, the vibration pattern of modes of *e* symmetry with frequencies 586, 590, 593, 597, 614, 618, 623, and 628 cm^{-1}.

mode behavior for the TO spectrum a and single mode behavior for the LO spectrum. The LO counterparts to the GaN confined modes are much weaker corresponding to their smaller and distributed oscillator strength.

The a_1-like infrared spectra are shown in Fig. 3. The vibration patterns of the strongest modes are shown in Fig. 4. In this case, we see a dominating TO mode at 570 cm^{-1}. This mode from Table II has a large bulklike LO-TO splitting

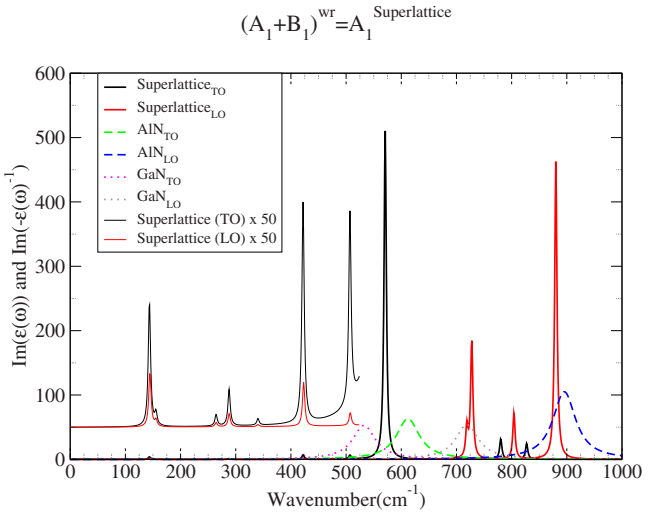

FIG. 3. (Color online) Longitudinal and transverse response of a_1-like phonon modes in $(AlN)_4(GaN)_4$ superlattice. Low-lying mode are multiplied by 50 for better viewing.

and the corresponding LO mode occurs at 718 cm^{-1}. These values are essentially GaN like but somewhat blueshifted because of the compressed GaN bonds. Looking at the corresponding mode eigenvector, however, we see that the mode involves in phase movements of all the N atoms in the entire cell both in the GaN and AlN part. The displacements of the N-atoms in the GaN part can be seen to be larger. Although we see slight displacements of the Al atoms rather than the Ga atoms, this is simply because the Ga atoms are heavier. So, we can still call this a mostly GaN A_1-type mode. We can discern two weaker TO peaks at 780 and 827 cm^{-1}. Their LO counterparts are clearly seen at 804 and 880 cm^{-1}. In fact, we find that the 827 cm^{-1} has a much stronger oscillator strength than the 848 cm^{-1} mode. Both these modes have larger N displacements in the AlN side of the cell although they also involve N motions in the GaN part of the cell. These modes are thus weakly confined to the AlN region. The common characteristic of these modes with strong oscillator strength is that they have several N atoms moving in phase with each other. The highest LO mode is still below that of pure AlN because of the strain effects. The mode at 754 cm^{-1} hardly has any oscillator strength at all in agreement with its negligible LO-TO splitting.

Interestingly, comparing a_1 and e modes, we found that the mode with highest LO-TO splitting for e symmetry is AlN like, while for a_1 it is GaN like. While for e modes, we found strong confinement-type effects mixed with localization near the interfaces; the a_1 modes have N displacements throughout the cell and are only weakly confined. Although there are many modes, only a few have strong coupling to the electric field because of the antiphase relation of the dipoles in most modes. The frequencies are substantially affected by the bond length changes relative to bulk GaN and AlN which occur because of our use of fully relaxed structures.

C. Variations with layer thickness

Experimentally, it is very difficult to control the layer thicknesses to a monolayer precision. It is thus of interest to examine how the above results change with layer thickness of the GaN and AlN parts of the cell. To this end we calculated the phonons and the infrared spectra of superlattices with the same total length but with either five GaN and three AlN layers or three GaN and five AlN layers. The superlattices were completely relaxed before the phonons were calculated. The relaxed lattice parameters a and c/a in the 4+4 superlattice are 5.90 Å and 1.618, which lies in between those of the $(GaN)_3(AlN)_5$ (3+5 for short) superlattice with

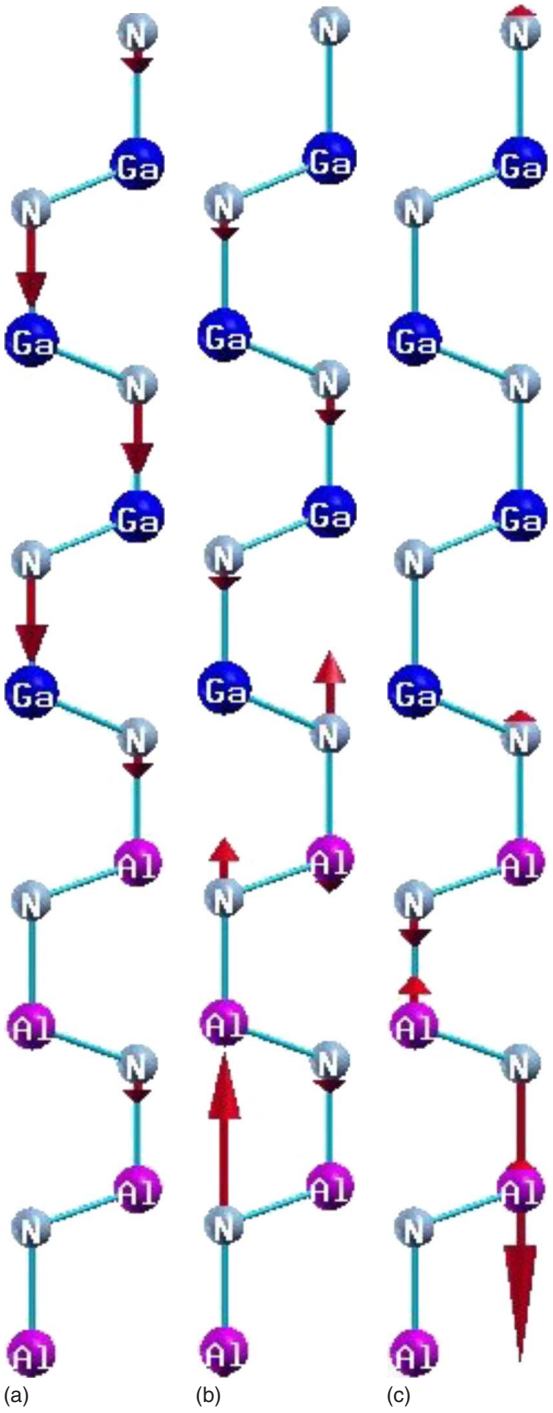

FIG. 4. (Color online) Eigenvector modes for the a_1 type optical modes with strongest oscillator strength, from left to right at frequencies 570, 780, and 827 cm^{-1}.

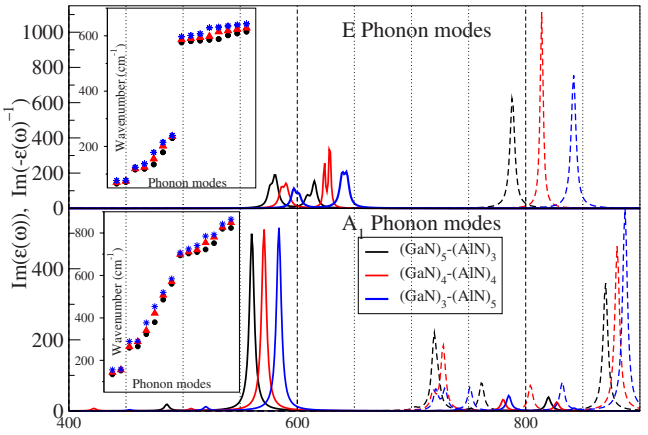

FIG. 5. (Color online) Comparison of phonons modes and infrared activity of e- and a_1-like phonon modes in $(GaN)_{8-n}(AlN)_n$, $(n=3,4,5)$ superlattices. The picture clearly shows that frequency increases with decreasing number of GaN layer or increasing AlN layer. The inset shows it is true for all phonons modes.

$a=5.86$ Å and $c/a=1.58$ and $(GaN)_5(AlN)_3$ 5+3 superlattice with $a=5.93$ Å and $c/a=1.620$.

The variation in the phonon frequencies and the IR spectra with the number of layers of AlN are shown in Fig. 5. In our fully relaxed supercells increasing the number of AlN layers number decreases the lattice constant a as well as the c/a ratio. Consequently the phonons frequencies have a general tendency to increase with number of AlN layers as show in Fig. 5.

D. Dielectric constants

As part of our study of the infrared spectra, we also obtain the dielectric tensor components in the static and high-frequency limit. The dielectric function tensor components are found to decrease with decreasing lattice constant or increasing AlN number of layers as shown in Table III. In this table we give both the high-frequency and the static dielectric constants. The high-frequency dielectric constant corresponds to the index of refraction squared in the visible region below the gap but above the phonon modes. The decrease in the high-frequency dielectric function is related to the increase in band gap with increasing AlN fraction in the cell. The effective gap of the superlattice is determined by the material with the lowest gap GaN; but the higher the AlN fraction, the shorter the GaN period and hence the higher the quantum confinement blueshift in this portion of the cell. We can also see that with increasing number of AlN layers, the anisotropy of the dielectric constants is increasing. It is not as clear why the static dielectric constants also should decrease with increasing AlN content. More ionic materials such as AlN could have a larger phonon contribution. However, the same trend is observed for the static as the high-frequency dielectric constant. Taking the differences between the static and high-frequency dielectric constants, we can see that the phonon contribution also decreases with increasing AlN layer thickness but less so than the high-frequency contribution.

TABLE III. High-frequency and static dielectric tensor components.

	$(GaN)_5(AlN)_3$	$(GaN)_4(AlN)_4$	$(GaN)_3(AlN)_5$
ϵ_{xx}^0	9.35	9.07	8.78
ϵ_{zz}^0	10.57	10.37	10.16
ϵ_{xx}^∞	5.32	5.10	4.88
ϵ_{zz}^∞	5.41	5.21	5.02

E. Comparison with experiment

A detailed comparison with experimental data given by Mintairov *et al.*[4] is encumbered by a number of factors. Our superlattices considered here are free-standing fully relaxed superlattices, while the experimental data correspond to superlattice layers grown on a buffer layer of GaN on sapphire. Thus the superlattices considered in the experiment are definitely in a different strain state from the idealized free-standing one considered here. Unfortunately, we have no full information on the strain state of the experimental superlattices. The experimental superlattices may also suffer from some statistical fluctuation in layer thickness around the nominal 4+4 superlattice.

Qualitatively, the experimental TO spectrum for e symmetry deduced from the reflectivity and shown in Fig. 5 of Ref. 4 shows also two peaks straddling 600 cm^{-1}. These are labeled as $E(TO1)$ and $E(TO2)$ and occur at about 580 and 640 cm^{-1}, respectively. These peaks show a wider separation experimentally than obtained in our calculation. Our lower peak is located at 590 cm^{-1}. The fact that ours is more blueshifted from pure GaN then the experimental one indicates that their lattice constant is closer to that of bulk GaN, which is consistent with the fact that they grow on a GaN buffer layer. Still, the experimental peak of GaN confined modes is higher than in bulk GaN. Our calculated $E(TO2)$ peak is at 628 cm^{-1}, lower than the experimental peak. We find this peak to be strongly interface localized but with a strong Al-N character. Correspondingly their peak position is closer to that of pure AlN although still below it. This indicates perhaps a more effective relaxation inside each four layer region of the experimental supercells. This could happen if misfit dislocations occur and release the biaxial strain from layer to layer.

Consistent with our calculations, the experimental data show essentially a single strong LO peak at about 840 cm^{-1}. We find that peak at 813 cm^{-1}. This is consistent with their AlN related $E(TO2)$ peak being closer to pure AlN than predicted by our fully relaxed but perfectly matched free-standing superlattice.

In conclusion, the comparison with the experimental data suggests that in the superlattices grown, individual AlN and GaN separately relax closer to bulklike lattice constants rather than being perfectly pseudomorphic and hence in a state of biaxial strain. In part this could also arise from small fluctuations in the layer number. As we saw above, if locally the system has a higher number of AlN layers, it will become more AlN like and this will shift the frequencies closer to pure AlN TO modes.

IV. CONCLUSIONS

We have calculated the phonons and infrared spectra of $(AlN)_n(GaN)_{8-n}$ superlattices with $n=3,4,5$ using first-principles calculations for fully relaxed free-standing structures. The infrared spectra were calculated and analyzed in comparison with the mode patterns. It was found that the spectra show essentially two TO peaks, one which corresponds to GaN confined modes and one corresponding to AlN confined modes. Interestingly, the GaN-like modes of e symmetry which correspond to in the basal plane vibrations consist of two closely spaced modes localizing near each interface but have relatively weak LO-TO splittings and no clearly visible LO peaks. The AlN confined modes give rise to two more clearly separated TO peaks but give rise to only one strong LO mode. For a_1 symmetry on the other hand, i.e., for vibrations parallel to the c-axis or superlattice direction, a GaN confined mode is the only one showing a strong LO-TO splitting. The a_1-type modes are less localized than the e-type modes. Clearly a rather complex interplay of the modes is at work in these systems which cannot be easily classified in terms of confined and interface modes.

The e-symmetry spectra are in qualitative agreement with a published experimental investigation.[4] However, there are discrepancies in frequency between our calculated and experimental results which are larger than those for the bulk compounds. This indicates that experimental superlattice is in a different strain state from our idealized perfectly matched and fully relaxed free-standing superlattice. In fact, these shifts could be viewed as a sensitive probe of the strain state of such superlattices. Our results indicate that the individual four layer units of GaN and AlN may to some extent separately relax toward their bulk values and are not perfectly constrained by the epitaxial relationship. This means that misfit dislocations or other strain relieve mechanisms may be operating in each individual four-layer unit. Among other this could contain fluctuations of the layer numbers. Thicker AlN layers will lead to frequencies closer to bulk AlN and thicker GaN layers will lead to frequencies closer to bulk GaN.

ACKNOWLEDGMENTS

We thank A. Mintairov for bringing his results to our attention and for useful discussions. This work was supported in part by ARO Grant No. W911NF-06-1-0476

[1] P. Y. Yu and M. Cardona, *Fundamentals of Semiconductors*, 2nd ed. (Springer, Berlin, 1999).
[2] O. Pagès, A. V. Postnikov, M. Kassem, A. Chafi, A. Nassour, and S. Doyen, Phys. Rev. B **77**, 125208 (2008).
[3] C. Bungaro, K. Rapcewicz, and J. Bernholc, Phys. Rev. B **61**, 6720 (2000).
[4] A. M. Mintairov, A. S. Vlasov, J. L. Merz, D. Korakakis, T. Moustakas, A. O. Osinsky, R. Gaska, and M. B. Smirnov, in *Wide-Bandgap Semiconductors for High-Power, High-Frequency, and High-Temperature Applications*, edited by S. Binari, A. Burk, M. M. Melloch, and C. Nguyen, MRS Symposia Proceedings No. 572 (Materials Research Society, Warrendale, PA, 1999), pp. 427–432.
[5] S. Baroni, P. Giannozzi, and A. Testa, Phys. Rev. Lett. **58**, 1861 (1987).
[6] X. Gonze, Phys. Rev. B **55**, 10337 (1997).
[7] X. Gonze and C. Lee, Phys. Rev. B **55**, 10355 (1997).
[8] M. C. Payne, M. P. Teter, D. C. Allan, T. A. Arias, and J. D. Joannopoulos, Rev. Mod. Phys. **64**, 1045 (1992).
[9] P. Hohenberg and W. Kohn, Phys. Rev. **136**, B864 (1964).
[10] W. Kohn and L. J. Sham, Phys. Rev. **140**, A1133 (1965).
[11] X. Gonze, J. M. Beuken, R. Caracas, F. Detraux, M. Fuchs, G. M. Rignanese, L. Sindic, M. Verstraete, G. Zerah, and F. Jollet, Comput. Mater. Sci. **25**, 478 (2002).
[12] J. P. Perdew and A. Zunger, Phys. Rev. B **23**, 5048 (1981).
[13] M. Fuchs and M. Scheffler, Comput. Phys. Commun. **119**, 67 (1999).
[14] K. Karch, J.-M. Wagner, and F. Bechstedt, Phys. Rev. B **57**, 7043 (1998).
[15] K. Karch and F. Bechstedt, Phys. Rev. B **56**, 7404 (1997).
[16] K. Karch, F. Bechstedt, and T. Pletl, Phys. Rev. B **56**, 3560 (1997).
[17] I. Gorczyca, N. E. Christensen, E. L. Peltzer y Blancá, and C. O. Rodriguez, Phys. Rev. B **51**, 11936 (1995).
[18] K. Kim, W. R. L. Lambrecht, and B. Segall, Phys. Rev. B **53**, 16310 (1996).
[19] K. Shimada, T. Sota, and K. Suzuki, J. Appl. Phys. **84**, 4951 (1998).
[20] L. E. McNeil, M. Grimsditch, and R. H. French, J. Am. Ceram. Soc. **76**, 1132 (1993).
[21] P. Perlin, A. Polian, and T. Suski, Phys. Rev. B **47**, 2874 (1993).
[22] L. Filippidis, H. Siegle, A. Hoffmann, C. Thomsen, K. Karch, and F. Bechstedt, Phys. Status Solidi B **198**, 621 (1996).